ASTRONOMY & ASTROPHYSICS
SUPPLEMENT SERIES

Astron. Astrophys. Suppl. Ser. **108,** 1-8 (1994)

Atomic data from the IRON Project. V. Effective collision strengths for transitions in the ground configuration of oxygen-like ions*

K. Butler[1] and C.J. Zeippen[2]

[1] Institut für Astronomie und Astrophysik der Universität München, Scheinerstraße 1, D-81679 München, Germany
[2] UPR 261 du CNRS et DAMAp and URA 173 (associée au CNRS et à l'Université Paris 7) et DAEC, Observatoire de Paris, F-92195 Meudon, France

Received March 3; accepted March 21, 1994

Abstract. — Fine-structure collision strengths for transitions between the ground configuration terms of oxygen-like ions have been obtained in a six state close-coupling approximation. Effective collision strengths are tabulated in the range of 1000–100000 K for the following ions: F II, Ne III, Na IV, Mg V, Al VI, Si VII, P VIII, S IX, Cl X, Ar XI.

Key words: atomic data — plasmas — infrared: ISM: lines

1. Introduction

Collisional cross sections are useful for astrophysical modelling but are particularly important in conditions found in nebulae (Osterbrock 1989) where the radiation field is not a dominating feature. Here, in spite of the low densities, collisional excitation is followed by radiative decay to produce the nebular emission lines. By comparing the strengths of pairs of lines, information concerning temperature, density and elemental abundances may be obtained. The accuracy of these determinations depends to a large extent on the input atomic data and thus it is desireable that these be as accurate as possible.

The launch of the IRAS satellite in 1983 opened up new possibilities since it was able to provide observations of infrared transitions between the levels of the ground configurations of a number of ions. These transitions are useful because the energy levels are close enough together that temperature effects are negligible. They thus represent excellent density diagnostics. The ISO satellite, with its improved instrumentation, will make more of these lines accessible for a larger number of astronomical objects.

This improvement in the observations presents a challenge to theoreticians, both from the point of view of the modelling and of the atomic parameters which the models require as input. The Iron Project (Hummer et al. 1994) has set itself the first goal of making such data available for all ions of interest. The paper of introduction just cited discusses the project, its aims and methods in full detail. This discussion will not be repeated here but we note that data have already been presented for ions in the carbon (Lennon & Burke 1994), boron (Zhang et al. 1994) and fluorine (Saraph & Tully 1994) isoelectronic sequences.

In this paper, the fifth in the series, we make available collisional data for oxygen-like ions. Previous work has been summarized and assessed by Pradhan & Gallagher (1993). With the exception of Ne III (Butler & Mendoza 1984) and Mg V (Mendoza & Zeippen 1987) only distorted wave calculations, which neglect resonance contributions, have been performed. Pradhan & Gallagher have judged the distorted wave results to be no more accurate than a factor of two. The present results use modern techniques which allow resonant contributions to be included accurately and they therefore represent a significant improvement over the earlier distorted wave results.

A brief description of the calculations, particularly those aspects specific to the ions at hand, is provided in the following section while the results are presented and compared with previous work in the third and final section.

2. Calculations

The collision rates have been obtained within a six-state close-coupling approximation in which the "target" ion consists of the $2p^4\ ^3P$, ^1D, ^1S, the $2s2p^5\ ^3P^o$, $^1P^o$ and the $2p^6\ ^1S$ terms plus a number of correlation config-

*The Tables are also available in electronic form: see the Editorial in A&A 1994 Vol. 280, No. 3, p. E1

Table 1. Observed and calculated F II, Ne III and Na IV target ion energies in cm^{-1}

F II	Obs.	Calc.	Ne III	Obs.	Calc.	Na IV	Obs.	Calc.
$2p^4\ ^3P^e_2$	0.0	0.0	$2p^4\ ^3P^e_2$	0.0	0.0	$2p^4\ ^3P^e_2$	0	0
$2p^4\ ^3P^e_1$	341.0	340.2	$2p^4\ ^3P^e_1$	642.9	637.2	$2p^4\ ^3P^e_1$	1106	1095
$2p^4\ ^3P^e_0$	489.9	490.2	$2p^4\ ^3P^e_0$	920.4	915.6	$2p^4\ ^3P^e_0$	1576	1565
$2p^4\ ^1D^e_2$	20873.4	21241.8	$2p^4\ ^1D^e_2$	25840.8	26101.3	$2p^4\ ^1D^e_2$	30840	31046
$2p^4\ ^1S^e_0$	44918.1	47294.6	$2p^4\ ^1S^e_0$	55750.6	57900.8	$2p^4\ ^1S^e_0$	66496	68575
$2s2p^5\ ^3P^o_2$	164797.9	168675.4	$2s2p^5\ ^3P^o_2$	204290.0	208768.9	$2s2p^5\ ^3P^o_2$	243682	249664
$2s2p^5\ ^3P^o_1$	165106.7	168998.5	$2s2p^5\ ^3P^o_1$	204876.0	209373.1	$2s2p^5\ ^3P^o_1$	244688	250698
$2s2p^5\ ^3P^o_0$	165279.2	169161.1	$2s2p^5\ ^3P^o_0$	205199.0	209678.3	$2s2p^5\ ^3P^o_0$	245239	251223
$2s2p^5\ ^1P^o_1$	239605.3	244417.6	$2s2p^5\ ^1P^o_1$	289479.0	299225.7	$2s2p^5\ ^1P^o_1$	343688	354386
$2p^6\ ^1S^e_0$	—	412112.7	$2p^6\ ^1S^e_0$	—	507714.2	$2p^6\ ^1S^e_0$	570823	604182

Table 2. Observed and calculated Mg V, Al VI and Si VII target ion energies in cm^{-1}

Mg V	Obs.	Calc.	Al VI	Obs.	Calc.	Si VII	Obs.	Calc.
$2p^4\ ^3P^e_2$	0.0	0.0	$2p^4\ ^3P^e_2$	0	0	$2p^4\ ^3P^e_2$	0	0
$2p^4\ ^3P^e_1$	1783.1	1762.4	$2p^4\ ^3P^e_1$	2732	2701	$2p^4\ ^3P^e_1$	4030	3976
$2p^4\ ^3P^e_0$	2521.8	2502.3	$2p^4\ ^3P^e_0$	3829	3797	$2p^4\ ^3P^e_0$	5565	5520
$2p^4\ ^1D^e_2$	35926.0	36098.3	$2p^4\ ^1D^e_2$	41167	41307	$2p^4\ ^1D^e_2$	46570	46714
$2p^4\ ^1S^e_0$	77279.0	79358.1	$2p^4\ ^1S^e_0$	88213	90337	$2p^4\ ^1S^e_0$	99341	101554
$2s2p^5\ ^3P^o_2$	283212.3	291501.2	$2s2p^5\ ^3P^o_2$	323002	334511	$2s2p^5\ ^3P^o_2$	363170	378939
$2s2p^5\ ^3P^o_1$	284828.3	293158.0	$2s2p^5\ ^3P^o_1$	325469	337032	$2s2p^5\ ^3P^o_1$	366786	382615
$2s2p^5\ ^3P^o_0$	285712.0	294004.3	$2s2p^5\ ^3P^o_0$	326815	338329	$2s2p^5\ ^3P^o_0$	368761	384526
$2s2p^5\ ^1P^o_1$	397482.0	410328.8	$2s2p^5\ ^1P^o_1$	451396	467362	$2s2p^5\ ^1P^o_1$	505650	525873
$2p^6\ ^1S^e_0$	662970.0	702010.3	$2p^6\ ^1S^e_0$	755628	801928	$2p^6\ ^1S^e_0$	849057	904558

Table 3. Observed and calculated P VIII, S IX and Cl X target ion energies in cm^{-1}

P VIII	Obs.	Calc.	S IX	Obs.	Calc.	Cl X	Obs.	Calc.
$2p^4\ ^3P^e_2$	0	0	$2p^4\ ^3P^e_2$	0	0	$2p^4\ ^3P^e_2$	0	0
$2p^4\ ^3P^e_1$	5760	5672	$2p^4\ ^3P^e_1$	7985	7872	$2p^4\ ^3P^e_1$	10880	10686
$2p^4\ ^3P^e_0$	7822	7750	$2p^4\ ^3P^e_0$	10648	10554	$2p^4\ ^3P^e_0$	14130	14006
$2p^4\ ^1D^e_2$	52256	52399	$2p^4\ ^1D^e_2$	58294	58417	$2p^4\ ^1D^e_2$	61000	64887
$2p^4\ ^1S^e_0$	110786	113172	$2p^4\ ^1S^e_0$	122700	125238	$2p^4\ ^1S^e_0$	130310	137952
$2s2p^5\ ^3P^o_2$	403803	425094	$2s2p^5\ ^3P^o_2$	444987	473211	$2s2p^5\ ^3P^o_2$	486850	523708
$2s2p^5\ ^3P^o_1$	408906	430277	$2s2p^5\ ^3P^o_1$	451995	480307	$2s2p^5\ ^3P^o_1$	496260	533188
$2s2p^5\ ^3P^o_0$	411736	433002	$2s2p^5\ ^3P^o_0$	455890	484090	$2s2p^5\ ^3P^o_0$	501510	538323
$2s2p^5\ ^1P^o_1$	560501	586199	$2s2p^5\ ^1P^o_1$	—	648642	$2s2p^5\ ^1P^o_1$	668850	713708
$2p^6\ ^1S^e_0$	943569	1010435	$2p^6\ ^1S^e_0$	1039219	1120187	$2p^6\ ^1S^e_0$	—	1234706

urations. This target had been previously used, in the context of the Opacity Project (Seaton et al. 1994), to obtain radiative data for members of the oxygen isoelectronic sequence (Butler & Zeippen 1994). The wavefunctions were obtained using the SUPERSTRUCTURE program of Eissner et al. (1974) in a version due to Nussbaumer & Storey (1978). The one-electron orbitals were optimized by minimizing the sum of the energies of the six states of interest. The properties of the target wavefunctions, energies and oscillator strengths etc. are discussed in full by Butler & Zeippen (1994). For present purposes it suffices to note the good agreement in the fine-structure energy levels shown in Tables ??–??, particularly for the levels of the ground configuration which are of relevance here. The observed energies (in cm^{-1}) have been taken from Bashkin & Stoner (1975) (F II, Ne III), Martin &

Zalubas (1981) (Na IV), Kaufman & Martin (1991) (Mg V), Martin & Zalubas (1979) (Al VI), Martin & Zalubas (1983) (Si VII), Martin et al. (1985) (P VIII), Martin et al. (1990) (S IX) and Bashkin & Stoner (1978) Cl X, Ar XI).

Table 4. Observed and calculated Ar XI target ion energies in cm^{-1}

Ar XI	Obs.	Calc.
$2p^4\ ^3P^e_2$	0	0
$2p^4\ ^3P^e_1$	14456	14230
$2p^4\ ^3P^e_0$	18274	18162
$2p^4\ ^1D^e_2$	71907	71914
$2p^4\ ^1S^e_0$	148513	151495
$2s2p^5\ ^3P^o_2$	529605	576940
$2s2p^5\ ^3P^o_1$	541976	589338
$2s2p^5\ ^3P^o_0$	548987	596179
$2s2p^5\ ^1P^o_1$	730452	781827
$2p^6\ ^1S^e_0$	—	1354663

The collisional problem itself was solved using the Opacity Project version of the R-matrix package as described by Berrington et al. (1987) together with an improved version of the asymptotic code due to Blum & Pradhan (1992). Sufficient partial waves were included to ensure convergence of the partial wave sum for these forbidden transitions. The energy mesh was set in terms of the effective quantum number relative to the next highest threshold to allow the resonances to be delineated adequately. Generally a step of 0.001 in the effective quantum number was used but at low energies this was reduced to 0.00025. This small step size is necessary to give good resolution of the near threshold resonances (see the figures).

The LS-coupling K-matrices were transformed algebraically to intermediate coupling before the collisional data were calculated. Thus relativistic effects were taken into account only in an approximate way. In particular, the differences in the energies of the levels was ignored. This is adequate for the ions considered here in which the fine-structure splitting is small. More highly ionized members of the sequence require a more accurate treatment. Work on these ions is in progress.

In the next section we discuss the accuracy of the present results with regard to this point and other deficiencies in the model.

3. Results

It is convenient to present collisional data in terms of the dimensionless collision strength Ω_{ij} which is related to the collisional cross section σ_{ij} via the relation

$$\Omega_{ij} = \frac{E}{\pi a_0^2}\sigma_{ij} \qquad (1)$$

a_0 being the Bohr radius and E the electron energy. Ω has the advantage that it is symmetric in the indices i, j. It is a complicated function of energy as can be seen in the figures making it unsuitable for presentation in tabular form. On the other hand, the effective collision strengths Υ are slowly varying functions of temperature and are to be found in Tables ??–?? for temperatures between 1000 and 100000 K. They result from a convolution of the collisional strengths Ω with a Maxwellian distribution,

$$\Upsilon = \int_0^\infty \Omega(x)\mathrm{e}^{-x}\mathrm{d}\,x. \qquad (2)$$

The variable x is the electron energy E in units of $k_\mathrm{B}T$, $x = E/k_\mathrm{B}T$, k_B being the Boltzmann constant and T the temperature. The downward rate coefficient from level j to i, q_{ji} is then given by

$$q_{ji} = \frac{8.631\ 10^{-6}}{T^{\frac{1}{2}}g_j}N_\mathrm{e}\Upsilon. \qquad (3)$$

The statistical weight of level j is g_j and N_e is the electron density. The upward rate may be found by detailed balancing arguments. The integration was performed using the analytical method of Burgess and Tully (1992), thereby ensuring correct behaviour of Υ in the low temperature limit.

The neglect of the energy splittings means that the resonance positions are slightly in error. Furthermore, the errors in the target energies, as evidenced by the tables, also introduce shifts in the positions of the resonances. While this is not serious for the higher energies (and temperatures) it can lead to larger errors when the resonances are large and close to threshold. This is illustrated in Figs. ?? and ?? where the $2p^4\ ^3P_0 - 2p^4\ ^3P_1$ transition in Ne III and Al VI are shown. For Ne III the positions of the resonances are not critical but the near threshold behaviour of the Al VI cross section is dominated by the resonant contribution. It is unfortunate that such low-lying resonances have not been observed for the ions of this sequence. Such observations would enable the collision rates to be determined more accurately. The only other alternative would be to perform a much more extensive calculation with many more target states included. However, Tables ??–?? indicate that the energies are of good accuracy giving some confidence in the present results.

The calculations at high energies also suffer from the limitation of the target to six states. Transitions with other higher-lying states, particularly with the continuum, are omitted together with resonances converging to these states. This means that the cross sections are underestimates at high energy. Again the solution would be a more extensive calculation. These omissions should not play a major rôle at the temperatures under consideration.

We turn now to a comparison of our results with those of previous authors. Given the accuracy of the wavefunctions as indicated by the good agreement with observed

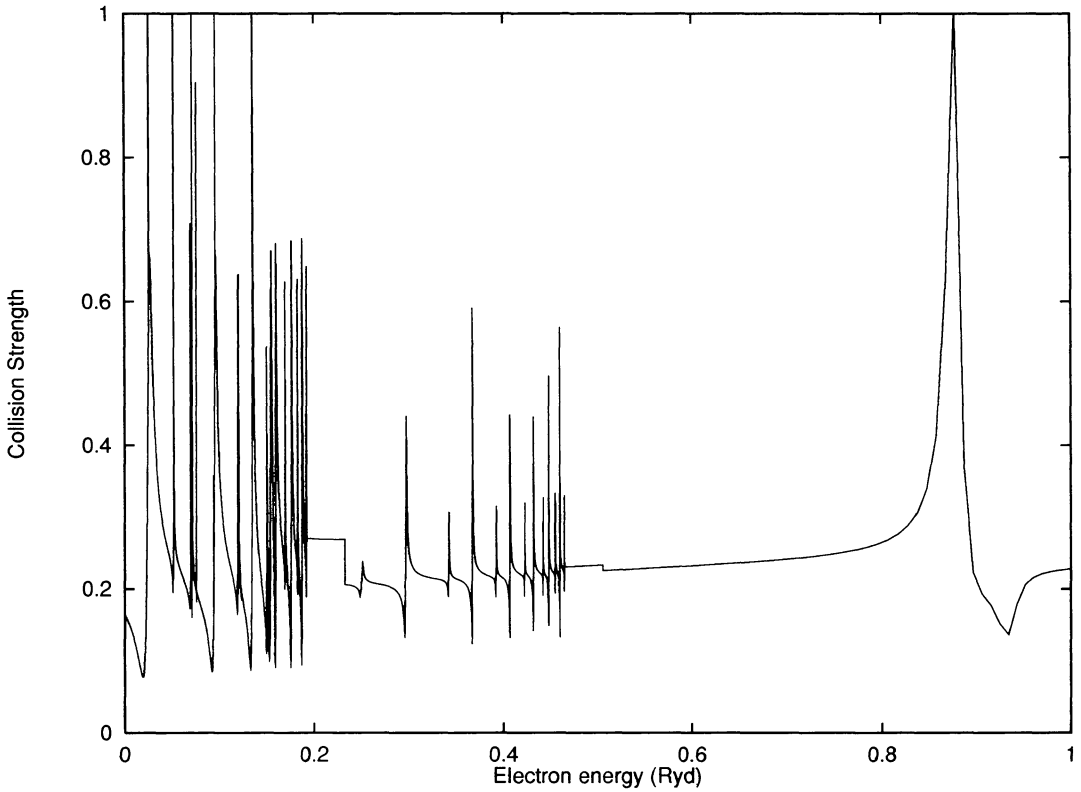

Fig. 1. Collision strength for the $2p^4\ ^3P_0$–$^3P_1$ transition in Ne III. The step in the cross section at 0.2 Ryd is due to the use of an averaging procedure

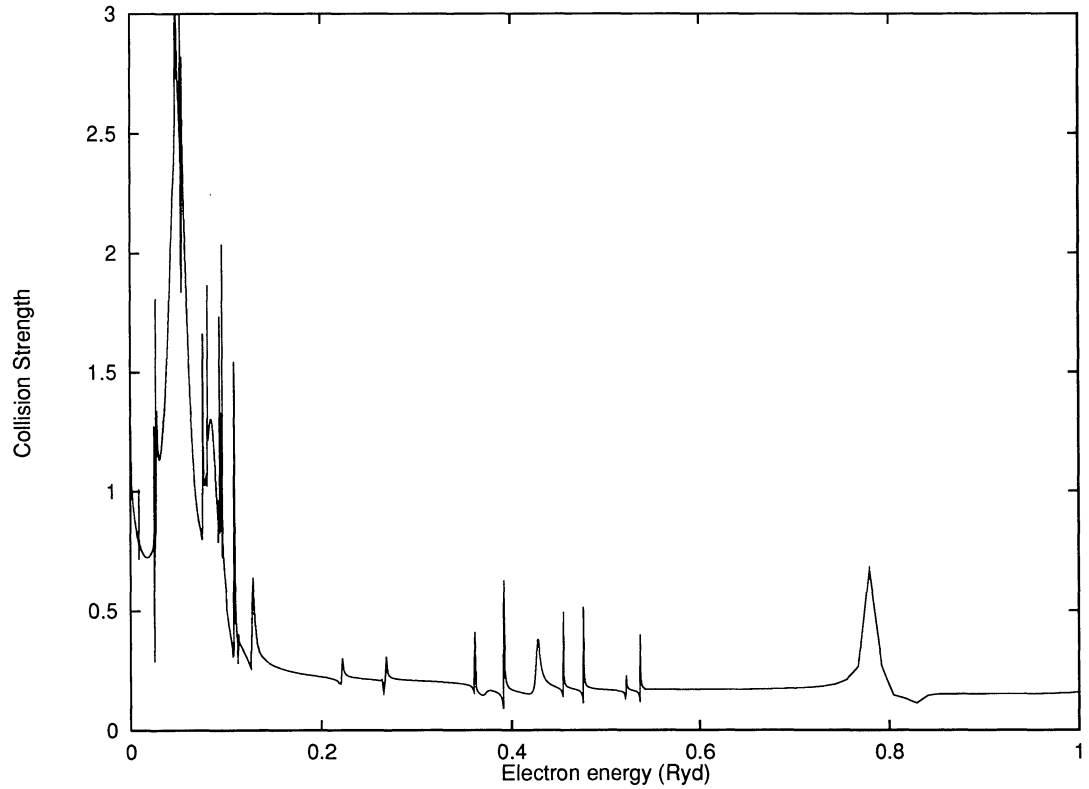

Fig. 2. Collision strength for the $2p^4\ ^3P_0$–$^3P_1$ transition in Al VI

Table 5. Effective collision strengths for F II as a function of $\log T$

	Transition									
$\log T$	$^3P_0$–$^3P_1$	$^3P_0$–$^3P_2$	$^3P_1$–$^3P_2$	$^3P_0$–^1D	$^3P_1$–^1D	$^3P_2$–^1D	$^3P_0$–^1S	$^3P_1$–^1S	$^3P_2$–^1S	^1D–^1S
3.0	.265	.174	.723	.154	.462	.771	.015	.044	.073	.363
3.2	.253	.166	.690	.149	.446	.744	.015	.044	.073	.362
3.4	.239	.158	.653	.142	.427	.712	.015	.044	.073	.361
3.6	.224	.151	.620	.137	.412	.687	.015	.044	.073	.358
3.8	.213	.150	.602	.135	.405	.675	.015	.044	.074	.354
4.0	.206	.152	.600	.135	.405	.675	.015	.045	.075	.348
4.2	.202	.156	.605	.137	.410	.683	.015	.046	.077	.342
4.4	.201	.160	.612	.140	.419	.699	.016	.047	.079	.338
4.6	.204	.165	.627	.145	.434	.724	.016	.049	.082	.339
4.8	.214	.175	.661	.152	.455	.758	.017	.052	.087	.347
5.0	.233	.191	.721	.160	.481	.801	.019	.056	.093	.358

energies and oscillator strengths (for the latter, see Butler and Zeippen 1994) we can expect our results to be good to roughly 10% in general. For Al VI the uncertainty in the positions of the resonances near threshold means that this cross section is less accurate than the rest of the present data. However, the increase in the rate compared to the distorted wave calculations certainly exists and will have implications for astrophysical modelling.

The overall accuracy is a great improvement over previous calculations except those for Ne III and Mg V which we discuss in more detail. Butler & Mendoza (1984) performed a four-state close-coupling calculation for Ne III based on the work of Pradhan (1976) while Mendoza & Zeippen (1987) used a five-state target for Mg V. The differences in the effective collision strengths for the ^3P transitions at 10000 K are 40% and 20% respectively. While the latter figure is within the combined error estimate of the two calculations the former is much larger. We note, however, that the present results are based on a more elaborate target and that many more energy points were used making the integration more accurate. Furthermore, the present results for the other transitions are in good agreement (to 10%) with those of Pradhan (1976). This gives us some confidence that our results are the more accurate in both these cases.

We thus conclude that our results are to be preferred for all ions of the sequence and that they have an accuracy of roughly 10% with the exception of those for Al VI. These last are, however, still the best results available to date.

Acknowledgements. We would like to express our gratitude to David Hummer who organizes the work of the Iron Project. This study is dedicated, in his 70th year, to Mike Seaton who guided our first steps in the field and has been a constant source of inspiration and motivation to several generations of atomic physicists. The calculations were performed on the Cray Y-MP of the Bayerische Akademie der Wissenschaft at the Leibniz-Rechen-Zentrum and were made possible by a grant of computer time from the Cray Corporation together with the LRZ.

References

Bashkin S., Stoner J.O.Jr. 1975, Atomic Energy Levels and Grotrian Diagrams Vol. I (North-Holland, Amsterdam)

Bashkin S., Stoner J.O.Jr. 1978, Atomic Energy-Level and Grotrian Diagrams Vol. II (North-Holland, Amsterdam)

Berrington K.A, Burke P.G., Butler K., Seaton M.J., Storey P.J., Taylor K.T., Yu Y. 1987, J. Phys. B: At. Mol. Phys. 20, 6379

Blum R.D., Pradhan A.K. 1992, ApJS 80, 425

Burgess A., Tully J.A. 1992, A&A 254, 436

Butler K., Mendoza C. 1984, MNRAS 208, 17P

Butler K., Zeippen C.J. 1994, J. Phys. B: At. Mol. Phys., in preparation

Eissner W. Jones M., Nussbaumer H. 1974, Comp. Phys. Commun. 8, 270

Hummer D.G., Berrington K.A., Eissner W., Pradhan A.K., Saraph H.E., Tully J.A. 1993, A&A 279, 298

Kaufman V., Martin W.C. 1991, J. Phys. Chem. Ref. Data 20, 121

Lennon D.J., Burke V.M. 1994, A&AS 103, 273

Martin W.C., Zalubas R. 1979, J. Phys. Chem. Ref. Data 8, 843

Martin W.C., Zalubas R. 1981, J. Phys. Chem. Ref. Data 10, 153

Martin W.C., Zalubas R. 1983, J. Phys. Chem. Ref. Data 12, 363

Martin W.C., Zalubas R., Musgrove A. 1985, J. Phys. Chem. Ref. Data 19, 786

Martin W.C., Zalubas R., Musgrove A. 1990, J. Phys. Chem. Ref. Data 19, 821

Mendoza C., Zeippen C.J. 1987, MNRAS 224, 7P

Nussbaumer H., Storey P.J. 1978, A&A 64, 139
Osterbrock D.E. 1989, Astrophysics of Gaseous Nebulae and Active Galactic Nuclei (University Science Books, Mill Valley, CA)
Pradhan A.K. 1974, J. Phys. B: At. Mol. Phys. 7, L503
Pradhan A.K., Gallagher J.W. 1993, At. Data Nucl. Data Tables 52, 227
Saraph H.E., Tully J.A. 1994, A&AS, in press
Seaton M.J.Yu.Y., Mihalas D., Pradhan A.K. 1994, MNRAS 266, 805
Zhang H.L, Graziani M., Pradhan A.K. 1994, A&AS 283, 319

Table 6. Effective collision strengths for Ne III as a function of $\log T$

	Transition									
$\log T$	$^3P_0$–$^3P_1$	$^3P_0$–$^3P_2$	$^3P_1$–$^3P_2$	$^3P_0$–^1D	$^3P_1$–^1D	$^3P_2$–^1D	$^3P_0$–^1S	$^3P_1$–^1S	$^3P_2$–^1S	^1D–^1S
3.0	.154	.128	.481	.150	.450	.749	.017	.050	.083	.266
3.2	.168	.149	.545	.153	.459	.765	.017	.050	.083	.266
3.4	.194	.174	.634	.154	.462	.771	.017	.050	.083	.266
3.6	.218	.194	.708	.153	.460	.767	.017	.050	.083	.266
3.8	.235	.204	.752	.152	.456	.760	.017	.050	.084	.267
4.0	.244	.208	.774	.151	.452	.754	.017	.050	.084	.269
4.2	.247	.208	.778	.150	.449	.749	.017	.050	.084	.277
4.4	.247	.205	.771	.149	.448	.746	.017	.051	.086	.292
4.6	.246	.203	.764	.150	.449	.749	.018	.054	.090	.310
4.8	.249	.205	.773	.153	.458	.763	.019	.057	.095	.325
5.0	.256	.211	.794	.156	.469	.782	.020	.060	.100	.333

Table 7. Effective collision strengths for Na IV as a function of $\log T$

	Transition									
$\log T$	$^3P_0$–$^3P_1$	$^3P_0$–$^3P_2$	$^3P_1$–$^3P_2$	$^3P_0$–^1D	$^3P_1$–^1D	$^3P_2$–^1D	$^3P_0$–^1S	$^3P_1$–^1S	$^3P_2$–^1S	^1D–^1S
3.0	.238	.178	.699	.122	.365	.609	.020	.061	.101	.208
3.2	.251	.194	.751	.123	.368	.614	.020	.060	.101	.208
3.4	.261	.202	.782	.123	.368	.613	.020	.060	.100	.208
3.6	.266	.203	.790	.121	.362	.603	.020	.060	.099	.208
3.8	.269	.202	.791	.119	.357	.595	.020	.059	.099	.208
4.0	.273	.205	.802	.122	.366	.610	.020	.059	.099	.211
4.2	.279	.213	.827	.130	.389	.649	.020	.060	.100	.218
4.4	.283	.221	.851	.139	.417	.695	.020	.061	.101	.227
4.6	.283	.225	.861	.147	.440	.733	.020	.061	.102	.239
4.8	.283	.233	.878	.151	.454	.756	.020	.061	.102	.254
5.0	.286	.250	.919	.153	.458	.763	.020	.061	.102	.271

Table 8. Effective collision strengths for Mg V as a function of $\log T$

	Transition									
$\log T$	$^3P_0$–$^3P_1$	$^3P_0$–$^3P_2$	$^3P_1$–$^3P_2$	$^3P_0$–^1D	$^3P_1$–^1D	$^3P_2$–^1D	$^3P_0$–^1S	$^3P_1$–^1S	$^3P_2$–^1S	^1D–^1S
3.0	.192	.116	.501	.145	.436	.727	.014	.042	.071	.181
3.2	.191	.121	.510	.144	.432	.720	.015	.045	.076	.182
3.4	.197	.136	.554	.144	.432	.720	.017	.050	.083	.182
3.6	.215	.163	.637	.145	.434	.723	.018	.054	.090	.182
3.8	.245	.197	.748	.145	.435	.726	.018	.055	.092	.181
4.0	.276	.225	.852	.146	.439	.732	.018	.055	.091	.182
4.2	.296	.240	.908	.148	.445	.742	.018	.053	.088	.186
4.4	.302	.246	.932	.148	.445	.742	.017	.051	.085	.199
4.6	.307	.262	.974	.145	.435	.726	.017	.050	.084	.221
4.8	.311	.284	1.029	.140	.421	.701	.017	.050	.084	.251
5.0	.311	.297	1.058	.135	.406	.676	.017	.050	.084	.278

Table 9. Effective collision strengths for Al VI as a function of $\log T$

	Transition									
$\log T$	$^3P_0$–$^3P_1$	$^3P_0$–$^3P_2$	$^3P_1$–$^3P_2$	$^3P_0$–^1D	$^3P_1$–^1D	$^3P_2$–^1D	$^3P_0$–^1S	$^3P_1$–^1S	$^3P_2$–^1S	^1D–^1S
3.0	0.950	2.011	5.713	0.133	0.400	0.666	0.010	0.030	0.049	0.258
3.2	0.936	1.899	5.442	0.136	0.409	0.682	0.010	0.030	0.051	0.301
3.4	0.993	1.856	5.419	0.135	0.405	0.676	0.011	0.034	0.056	0.366
3.6	1.081	1.833	5.475	0.133	0.398	0.663	0.013	0.039	0.065	0.418
3.8	1.111	1.725	5.271	0.130	0.390	0.650	0.015	0.044	0.074	0.429
4.0	1.041	1.498	4.673	0.126	0.378	0.631	0.016	0.047	0.078	0.417
4.2	0.897	1.204	3.831	0.121	0.363	0.606	0.016	0.048	0.080	0.425
4.4	0.730	0.914	2.969	0.116	0.348	0.580	0.016	0.048	0.081	0.463
4.6	0.578	0.675	2.242	0.112	0.336	0.561	0.016	0.048	0.080	0.487
4.8	0.462	0.504	1.711	0.110	0.329	0.548	0.016	0.047	0.079	0.471
5.0	0.381	0.395	1.365	0.107	0.322	0.537	0.015	0.046	0.077	0.427

Table 10. Effective collision strengths for Si VII as a function of $\log T$

	Transition									
$\log T$	$^3P_0$–$^3P_1$	$^3P_0$–$^3P_2$	$^3P_1$–$^3P_2$	$^3P_0$–^1D	$^3P_1$–^1D	$^3P_2$–^1D	$^3P_0$–^1S	$^3P_1$–^1S	$^3P_2$–^1S	^1D–^1S
3.0	.133	.066	.314	.164	.493	.821	.011	.034	.057	.088
3.2	.141	.074	.344	.157	.472	.787	.011	.034	.057	.089
3.4	.154	.084	.383	.148	.445	.742	.012	.035	.058	.089
3.6	.167	.092	.417	.138	.414	.689	.013	.038	.063	.090
3.8	.176	.098	.441	.127	.381	.636	.014	.041	.069	.091
4.0	.182	.104	.461	.117	.352	.587	.015	.044	.073	.092
4.2	.188	.112	.485	.110	.329	.548	.015	.044	.074	.094
4.4	.192	.122	.514	.103	.310	.517	.014	.043	.071	.097
4.6	.199	.138	.558	.099	.296	.493	.014	.041	.068	.106
4.8	.208	.163	.627	.095	.284	.474	.013	.039	.065	.123
5.0	.217	.188	.695	.091	.274	.457	.012	.037	.062	.149

Table 11. Effective collision strengths for P VIII as a function of $\log T$

	Transition									
$\log T$	$^3P_0$–$^3P_1$	$^3P_0$–$^3P_2$	$^3P_1$–$^3P_2$	$^3P_0$–^1D	$^3P_1$–^1D	$^3P_2$–^1D	$^3P_0$–^1S	$^3P_1$–^1S	$^3P_2$–^1S	^1D–^1S
3.0	.146	.089	.384	.073	.218	.363	.010	.029	.048	.091
3.2	.149	.093	.395	.075	.224	.373	.010	.029	.048	.091
3.4	.158	.107	.438	.078	.234	.391	.010	.029	.048	.091
3.6	.182	.137	.536	.082	.246	.410	.010	.029	.049	.091
3.8	.223	.173	.668	.084	.253	.422	.010	.030	.050	.094
4.0	.263	.200	.778	.085	.254	.423	.010	.031	.051	.100
4.2	.292	.217	.853	.083	.249	.415	.010	.031	.052	.110
4.4	.308	.243	.931	.081	.242	.403	.010	.031	.052	.125
4.6	.309	.274	1.002	.079	.236	.393	.010	.031	.052	.147
4.8	.294	.287	1.014	.077	.230	.384	.010	.031	.052	.177
5.0	.268	.278	.960	.075	.225	.375	.010	.031	.051	.259

Table 12. Effective collision strengths for S IX as a function of $\log T$

	Transition									
$\log T$	$^3P_0$–$^3P_1$	$^3P_0$–$^3P_2$	$^3P_1$–$^3P_2$	$^3P_0$–^1D	$^3P_1$–^1D	$^3P_2$–^1D	$^3P_0$–^1S	$^3P_1$–^1S	$^3P_2$–^1S	^1D–^1S
3.0	0.244	0.263	0.892	0.204	0.611	1.018	0.008	0.024	0.040	0.085
3.2	0.270	0.425	1.290	0.207	0.622	1.036	0.008	0.024	0.040	0.086
3.4	0.346	0.723	2.053	0.194	0.582	0.970	0.008	0.024	0.040	0.086
3.6	0.444	0.993	2.785	0.168	0.503	0.838	0.008	0.024	0.039	0.088
3.8	0.503	1.082	3.059	0.137	0.412	0.687	0.008	0.024	0.039	0.092
4.0	0.501	0.990	2.850	0.111	0.333	0.556	0.008	0.024	0.040	0.111
4.2	0.459	0.809	2.392	0.092	0.277	0.461	0.008	0.025	0.041	0.163
4.4	0.404	0.619	1.894	0.081	0.242	0.403	0.009	0.026	0.043	0.236
4.6	0.346	0.458	1.461	0.074	0.223	0.372	0.009	0.027	0.044	0.290
4.8	0.293	0.340	1.129	0.071	0.214	0.357	0.009	0.027	0.044	0.302
5.0	0.251	0.264	0.907	0.070	0.209	0.348	0.009	0.026	0.043	0.283

Table 13. Effective collision strengths for Cl X as a function of $\log T$

	Transition									
$\log T$	$^3P_0$–$^3P_1$	$^3P_0$–$^3P_2$	$^3P_1$–$^3P_2$	$^3P_0$–^1D	$^3P_1$–^1D	$^3P_2$–^1D	$^3P_0$–^1S	$^3P_1$–^1S	$^3P_2$–^1S	^1D–^1S
3.0	.096	.048	.229	.045	.135	.225	.004	.013	.022	.066
3.2	.096	.048	.229	.045	.135	.225	.005	.014	.024	.064
3.4	.096	.048	.229	.045	.135	.225	.005	.016	.026	.060
3.6	.096	.049	.230	.045	.135	.224	.006	.017	.028	.056
3.8	.098	.050	.236	.045	.135	.226	.006	.018	.030	.053
4.0	.105	.055	.255	.047	.140	.233	.006	.018	.030	.050
4.2	.123	.063	.295	.050	.149	.248	.006	.018	.030	.049
4.4	.147	.075	.352	.053	.158	.264	.006	.018	.031	.050
4.6	.168	.092	.417	.054	.163	.272	.006	.018	.031	.055
4.8	.182	.118	.493	.054	.162	.271	.006	.019	.031	.072
5.0	.187	.148	.568	.053	.158	.264	.006	.019	.032	.102

Table 14. Effective collision strengths for Ar XI as a function of $\log T$

	Transition									
$\log T$	$^3P_0$–$^3P_1$	$^3P_0$–$^3P_2$	$^3P_1$–$^3P_2$	$^3P_0$–^1D	$^3P_1$–^1D	$^3P_2$–^1D	$^3P_0$–^1S	$^3P_1$–^1S	$^3P_2$–^1S	^1D–^1S
3.0	.083	.048	.212	.039	.116	.194	.005	.016	.026	.049
3.2	.084	.050	.219	.039	.116	.194	.005	.016	.026	.049
3.4	.087	.055	.232	.039	.116	.194	.005	.016	.026	.049
3.6	.092	.061	.251	.039	.117	.195	.005	.016	.026	.049
3.8	.099	.070	.281	.040	.119	.198	.005	.016	.026	.049
4.0	.111	.083	.325	.041	.123	.204	.005	.016	.026	.050
4.2	.131	.097	.382	.042	.127	.211	.005	.016	.026	.051
4.4	.160	.115	.459	.043	.129	.214	.005	.016	.026	.055
4.6	.190	.139	.551	.043	.128	.213	.005	.016	.026	.064
4.8	.207	.161	.621	.042	.125	.209	.005	.016	.027	.079
5.0	.206	.170	.639	.041	.123	.206	.006	.017	.028	.097